UNIVERSITY OF CALIFORNIA, SAN DIEGO

Fabrication of Anodic Aluminum Oxide Membrane for High Heat Flux Evaporation

A Thesis submitted in partial satisfaction of the requirements for the degree Master of Science

in

Mechanical Engineering

by

Kristine McGrath

Committee in Charge:

Professor Renkun Chen, Chair
Professor Carlos Coimbra
Professor Olivia Graeve

2016

The Thesis of Kristine McGrath is approved and it is acceptable in quality and form for publication on microfilm and electronically:

Chair

University of California, San Diego

2016

TABLE OF CONTENTS

LIST OF FIGURES

ACKNOWLEDGEMENTS

I would like to thank my thesis advisor Dr. Renkun Chen for his support and guidance on this project. I would like to thank Young Kim and Qingyang Wang who also worked on this project and without their help and contribution this project would not be where it is today. I would also like to thank my family and friends for their support.

Sections 2-4 are currently being prepared for submission for publication of the material. Kim, Young Jin; Wang, Qingyang; McGrath, Kristine; Chen, Renkun. The thesis author was a co-author of this material.

ABSTRACT OF THE THESIS

Fabrication of Anodic Aluminum Oxide Membrane for High Heat Flux Evaporation

by

Kristine McGrath

Master of Science in Mechanical Engineering

University of California, San Diego, 2016

Professor Renkun Chen, Chair

As electronics become more powerful and have higher energy densities, it is becoming more and more necessary to find solutions to dissipate these high heat fluxes. One promising solution to this problem is nanopore evaporative cooling. However, based on current literature, the experimental data is far below what is expected from the theoretical calculations.

In this thesis, the experimental results produced heat fluxes much closer to the theoretical values. Experimentally, a maximum heat dissipation of 103 W was

achieved on a $0.5\ cm^2$ area which corresponds to a heat flux of $206\ W/cm^2$ on the overall AAO surface or a heat flux of $\sim 400\ W/cm^2$ on the active evaporating pore area which is close to the theoretical heat flux of $572\ W/cm^2$ that can be obtained given the membrane parameters. While the results are promising, it still needs to be further studied to obtain higher heat fluxes closer to the theoretical one. In order to achieve this, membrane parameters of the working porous membrane need to be able to be adjusted.

For the nanopore evaporative experiments done so far, commercially available AAO membranes were used. However, commercial AAO is only sold in certain set parameters and the AAO produced has a disordered structure, both of which are not useful for future experimental purposes. Therefore, AAO needs to be fabricated in the lab to meet the experimental needs.

The fabrication of AAO on high purity aluminum (99.997%) with 0.3 M Oxalic Acid at 40 V at $6 - 7℃$ was achieved. With the given fabrication parameters an average pore size of ~80 nm was achieved with a circularity of 0.91 while the commercial AAO had an average pore size of ~200 nm with a circularity of 0.80.

The initial nanopore evaporative cooling experiments will be discussed along with the process of fabricating usable AAO for these experiments.

I. Introduction

I.I Motivation

As electronics become more powerful and have higher energy densities, it is becoming more and more necessary to find solutions to dissipate high heat fluxes. Current heat dissipation technology is a limiting factor for these high powered electronics such as integrated circuits, processors, and laser diodes [6-7]. These high powered electronics can have overall heat fluxes of $100\ W/cm^2$ and concentrated local hot spots that can exceed $500\ W/cm^2$ [13]. In order to keep up with these high energy density technologies it is imperative to improve the thermal management of these devices. This research is necessary due to the fact that performance and reliability are negatively affected by these high temperatures [11].

Traditional cooling techniques that have been used for electronics are conduction through thermal stacks, convection of air with the help of fans, and heat sinks [7,11]. These techniques have worked for current lower powered electronics but they are limited by their size, weight, and power. Therefore, research in thermal management has been taken on in applications such as jet impingement [34], pool boiling [12], phase change materials (PCMs) [11], and thin film evaporation [6-7,11-12,34].

I.II Nanopore Evaporative Cooling and the Use of AAO

Nanopore evaporative cooling is a solution for thermal management. However, it still needs to be further researched in order to be a viable option. Based on the current experimental data, it is far below what has been predicted in theoretical calculations causing doubts to arise regarding the feasibility of this idea. To better understand and model nanopore evaporation, AAO is used as the working porous membrane and IPA is used as the working fluid. IPA was chosen because of its high wettability on AAO and its dielectric properties.

I.III Thesis Objectives

For the nanopore evaporative cooling experiments achieving a higher heat flux than has been achieved in literature and on a larger area thus far is the goal. To begin with, experiments will be similar to those done in literature, using the same working fluid (IPA) and nanoporous membrane (AAO) to be able to make a direct comparison. To begin with, these experiments will use commercially produced AAO from Whatman. However, commercially purchased AAO has a limited variety of options to choose from and is not very ordered.

For future nanopore evaporative cooling experiments AAO fabricated in the lab is desired due to the fact that parameters such as pore diameter, membrane thickness, porosity, and pore ordering can be better controlled. To do this, designing a

set-up and fine-tuning the process of producing generic AAO is necessary before adjusting the parameters is done.

This thesis will cover the theory, setup, and execution of nanopore evaporative cooling experiments. It will then discuss the fabrication parameters that affect the AAO membranes, the setup for fabricating usable AAO for experiments, and how well the results compare to not only the commercially produced AAO but the AAO parameters that are desired for nanopore evaporative cooling experiments.

II.Nanopore Evaporative Cooling

II.I Introduction

Nanopore evaporative cooling is a design that takes advantage of evaporative heat transfer to dissipate heat. It uses a thin porous membrane supported by microchannels which supply liquid to the nanopores by capillary pressure as shown in **Figure 1** [7]. Based on current experimental data, however, it is far below what has been predicted in theoretical calculations. The highest heat flux dissipated using IPA as the working fluid was $\sim 96\, W/cm^2$ achieved by Xiao et al [6].

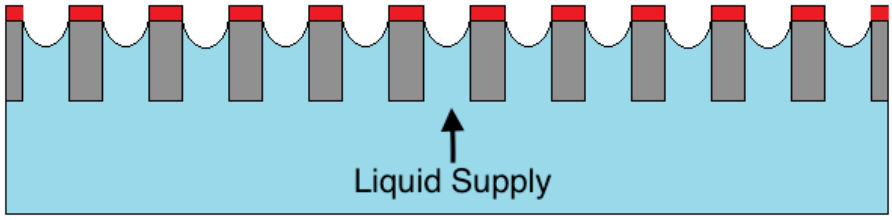

Figure 1: The nanopore evaporative cooling membrane schematic.

There are several experiments that have achieved heat fluxes close to 1 kW/cm^2 but they have only been achieved in experiments that either had a wall superheat that is very large [32] or occurred on a heating area that is very small [13,31]. Both of these configurations are not practical which is why further research still needs to be done.

Important parameters that significantly affect the performance and the amount of heat dissipation during the evaporation are the capillary radius/pore diameter, the

temperature of the pore wall, and the degree of saturation of the vapor phase [9]. The meniscus also plays an important role in evaporation and the heat dissipation process.

II.II The Meniscus

The meniscus plays an important role in dissipating heat in thin film evaporation. Therefore, a better understanding of the meniscus can lead to a better understanding of evaporation in nanopores and this knowledge can be used to achieve higher heat flux dissipation by designing nanoporous membranes that reflect favorable conditions. The meniscus can be analyzed in two regards: the location of the meniscus within a nanopore and the regions that make up the meniscus itself.

Looking at the meniscus location within a nanopore, the meniscus can be categorized into three locations: (1) pinning regime, (2) fully extended meniscus, and (3) receding meniscus [14], which can be seen in **Figure 2**.

The pinning regime occurs at low superheats. In this region, the liquid-vapor interface changes in size and curvature depending on the different conditions such as the liquid supply pressure and the temperature of the pore wall.

As the superheat increases, the meniscus increases in length until it becomes fully extended. Here the liquid-vapor interface is at its maximum pressure difference.

As the superheat continues to increase, the meniscus begins to recede within the nanopore. As the meniscus recedes further into the pore, the probability of the

vapor molecules escaping becomes lower, making heat dissipation less efficient. This is one of the reasons why the thickness of the membrane should be thin.

As the superheat becomes more extreme, the meniscus will eventually each the bottom of the pore resulting in dry out. This is undesirable since evaporation is no longer able to occur within the pores and the heat is no longer being adequately dissipated causing the membrane to overheat and potentially break.

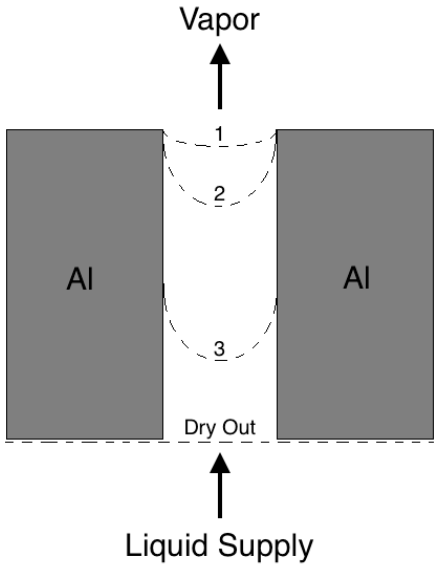

Figure 2: Meniscus locations within a pore. 1: The pinning regime. 2: Fully extended meniscus. 3: Receding meniscus.

The meniscus can also be further analyzed by looking at the distinct regions that make up the meniscus. For an evaporating meniscus with perfect wetting conditions, it can be broken down into three regions: (1) adsorber film, (2) transition, and (3) bulk meniscus [8] as seen in **Figure 3**.

In the adsorber film region, the meniscus has a uniform thickness and evaporation is unable to occur due to the large attractive forces between the solid-liquid interface, vapor pressure, and pore wall temperature [8]. Here the heat flux is ~0 and does not play an active role in heat dissipation.

The next region that makes up the meniscus is the transition region. Here the attractive forces between the solid-liquid interface are much weaker and is where the meniscus starts taking on curvature. It is in this region that the strongest evaporation and therefore the highest heat flux occurs. Because this is where most of the heat is being dissipated, this is the region of the meniscus that needs to be optimized for future nanopore evaporative cooling.

The final region of the meniscus is the bulk meniscus. It is in this region that the curvature is nearly constant and it serves as the liquid supply for the transition region.

Beyond the tip of the meniscus is the liquid supply. This region can be categorized and modeled by the Hagen-Poiseuille equation.

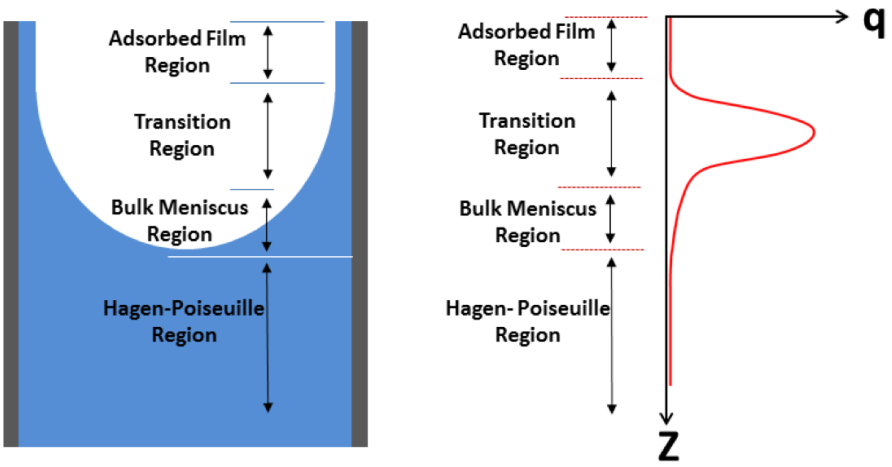

Figure 3: Regions that make up the meniscus. Region 1: Adsorbed film. Region 2: Transition. Region 3: Bulk meniscus. Beyond the tip of the meniscus is the Hagen-Poiseuille region where the liquid supply is located.

By having a better understanding of the meniscus and where the liquid is being evaporated from, nanoporous membranes can be made to better suit favorable conditions for evaporation. By knowing that evaporation is less favorable the further the meniscus is within the pore, nanoporous membranes can be designed to be thinner rather than thicker to improve results and prevent dry out from occurring as rapidly. By knowing that the transition region in a meniscus is where the highest evaporation occurs, membranes can be designed to alter the pore diameter to get a better understanding of how the pore diameter affects the meniscus and the size of this area to see the pore size at which this region is optimized.

II.III Nanopore Membrane for Evaporative Cooling

The nanopore membrane plays an important role in this evaporative heat transfer design. The membrane thickness, pore diameter, and porosity of the AAO all play a role in how well the liquid is able to evaporate and the heat is able to dissipate. Higher porosities and thinner membranes are desired to increase heat dissipation [6].

Section II is currently being prepared for submission for publication of the material. Kim, Young Jin; Wang, Qingyang; McGrath, Kristine; Chen, Renkun.

III.Experimental Design for Nanopore Evaporative Cooling

III.I Theoretical Critical Heat Flux

The theoretical critical heat flux can be found using the liquid transport limit or the kinetic limit for evaporation. Depending on the configuration and experimental parameters, either can be the limiting factor which is why both values have to be calculated to determine which produces a lower heat flux. The one that does is the true limiting factor for the configuration and the maximum theoretical critical heat flux that can be achieved.

The liquid inside the pores is driven by both the capillary force as well as the pressure difference of ~100 kPa across the membrane, with the flow facing resistance from the pore wall. The critical heat flux for the liquid transport being the limiting factor can be calculated as the value at which the liquid feed force and the viscous drag force are balanced. At this point, the meniscus is fully extended and the curvature of the liquid-vapor interface has a value similar to the inverse of the pore radius due to the fact that IPA has ~0° angle with AAO. Therefore, the liquid transport driven pressure can be calculated by:

$$\Delta P_{dri} = \frac{4\gamma}{D} + 101.325kPa$$

Where D is the pore diameter, γ is the liquid surface tension, and the 101.325 kPa is the pressure difference between the liquid reservoir at 1 atm and vacuum chamber which also plays a role in the liquid driving force. For the experiments, the membrane

pore diameter is ~200 nm and the liquid surface tension for IPA is $21.4\times10^{-3}\ N/m$ which comes out to a value of $\Delta P_{dri} = 529\ kPa$.

Assuming that the density of IPA stays constant, the viscous pressure drop inside the pore can be calculated using the Hagen-Poiseuille equation:

$$\Delta P_{vis} = \frac{32\mu L v}{D^2} = \frac{32\mu L}{D^2}\frac{q''}{h_{fg}\rho_l}$$

Where μ is the liquid viscosity, ρ_l is the liquid density, h_{fg} is the latent heat of evaporation, L is the pore length or membrane thickness, and q'' is the heat flux. For IPA under atmospheric conditions, the viscosity is $1.33\times10^{-3} Pa\cdot s$, the density is $786\ \ kg/m^3$, and the latent heat of evaporation is $732\ \ kJ/kg$. The pore length or membrane thickness is 50 μm.

When $\Delta P_{dri} = \Delta P_{vis} = 529\ kPa$, that is the maximum critical heat flux that can be achieved. This corresponds to a heat flux of $q'' = 572\ \ W/cm^2$, if the liquid transport is the limiting factor in this situation.

The other limiting factor could be the kinetic limit for evaporation which can be calculated using the equation [33]:

$$q'' = \frac{2\sigma}{2-\sigma} h_{fg}\sqrt{\frac{M}{2\pi R}}\left(\frac{p_{l,corr}}{\sqrt{T_l}} - \frac{p_v}{\sqrt{T_v}}\right)$$

Where σ is the accommodation coefficient of the liquid, M is the molar mass of the liquid, R is the gas constant, p_v is the far field pressure of the vapor, T_v is the far field temperature of the vapor, T_l is the temperature of the liquid near the liquid-vapor

interface, and $p_{l,corr}$ is the corrected pressure of the liquid near the liquid-vapor interface. $p_{l,corr}$ can be calculated with the Kelvin's equation for pressure change at a curved liquid-vapor interface:

$$p_{l,corr} = p_l \times exp\left(-\frac{2\gamma M}{rR\rho_l T_l}\right)$$

Here p_l is 101.325 kPa based on the experimental set-up and the accommodation coefficient is 0.1. This results in a critical heat flux of $q'' \approx 1400\, W/cm^2$ which is higher than the critical heat flux obtained from the liquid transport. Therefore, the liquid transport is the limiting factor in this setup and the maximum theoretical critical heat flux is $q'' = 572\ W/cm^2$.

III.II Evaporative Cooling Experiment Set-up

The AAO membrane was attached on top of a 71mm x71mm square hole in a PMMA block using Torr Seal ® Low Pressure epoxy. Due to the fact that the membrane was bigger than the hole in the PMMA, part of the pores were blocked by the PMMA and epoxy making them inactive for evaporation.

Once the epoxy was set, a shadow mask with a 0.5 cm^2 area opening was used to deposit a 2-3 nm thick layer of Chrome on the top of the membrane using PVD (Physical Vapor Deposition) as an adhesive layer. Next a 30 nm thick layer of Platinum was deposited on top to act as the heater for the system.

Using a second mask, copper contact pads with a thickness of 2 μm are deposited. The internal resistance of the contact pads are less than 0.1 ohm.

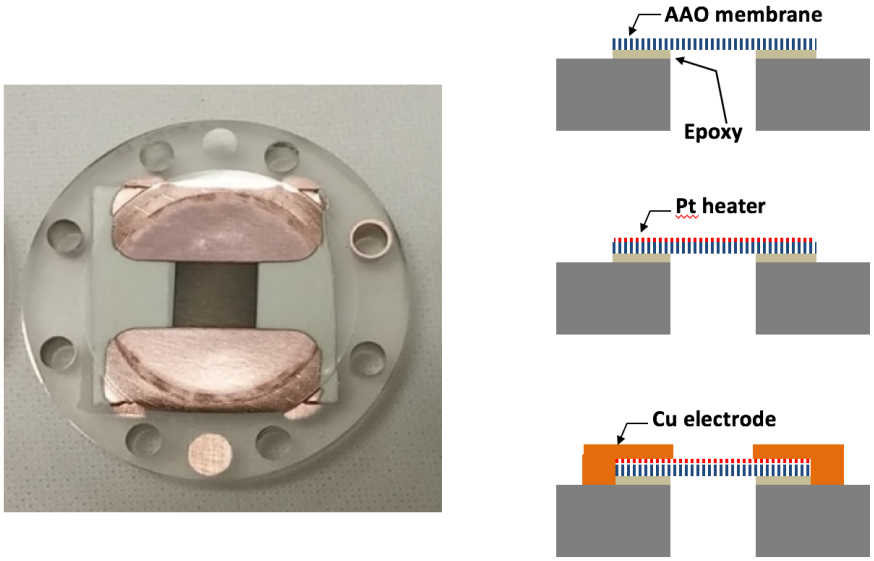

Figure 4: Overview of the membrane assembly.

III.III Temperature Sensor Calibration

In order to determine the temperature the AAO membrane was experiencing in experiments, the AAO sample with the Platinum layer was calibrated by measuring how the membrane's resistance varied with temperature to determine its temperature coefficient of resistance (TCR). This calibration was done using a programmable convection oven and a thermocouple.

An electrical connection was made on both sides of the copper electrode in order to measure the resistance and the thermocouple was placed less than 1mm above

the membrane in order to measure the temperature of the membrane as close as possible without introducing error via conduction from touching. The resistance and temperature of the Platinum was recorded using the Agilient 34401A multimeter and the NI USB-TC01 data acquisition.

The measurements began at room temperature and went up to 50℃. The temperature was increased in 5K increments, holding each temperature for two and a half hours before taking the measurement so that the heater could come to an equilibrium temperature and resistance. The data was then plotted as shown in **Figure 5** and the TCR value was found by taking the slope of the plot. The membrane was calibrated with a TCR value of $0.0011/K$.

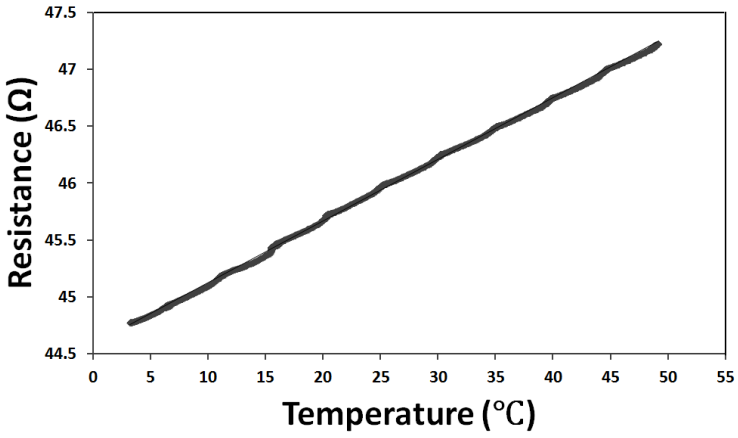

Figure 5: Temperature vs Resistance of the membrane. Used to determine the temperature coefficient of resistance (TCR).

III.IV Experimental Set-up

The completed membrane assembly was attached to the liquid supply channel using an O-ring seal to prevent leaking and set screws to hold it into place. Once the liquid supply channel was securely attached to the membrane assembly, the electrical connections were attached.

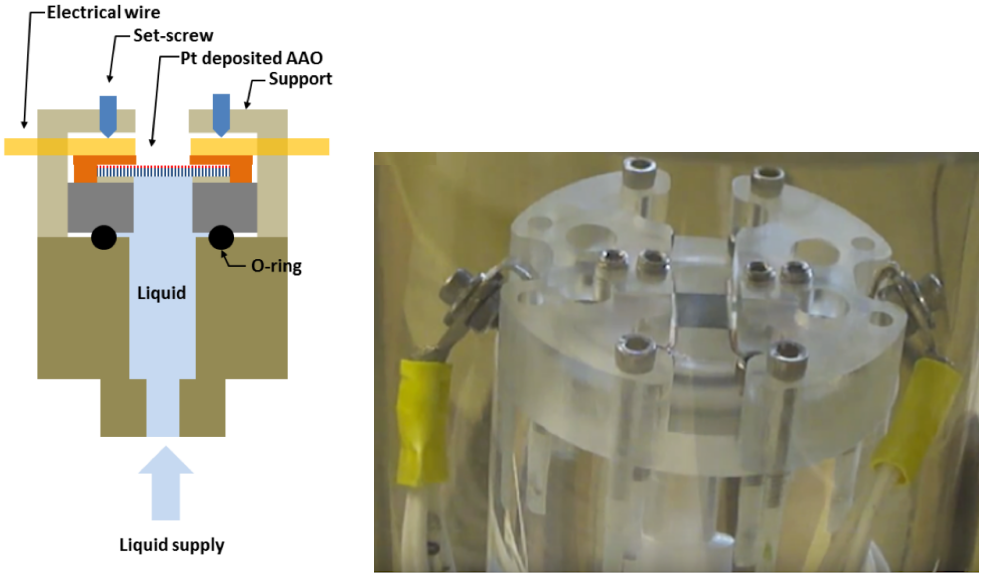

Figure 6: Membrane assembly and liquid supply channel set-up

After the electrical connections were all set up, a glass case was placed over the entire set-up and on to the platform using an O-ring to seal the set-up. Once secure, the vacuum was turned on and the pressure within the chamber is reduced to ~3 Pa. Once the pressure had been stabilized, the liquid supply was slowly introduced into the membrane assembly using the valve to control the flow and not break the membrane in the process. At this point the pressure was now around 40 Pa.

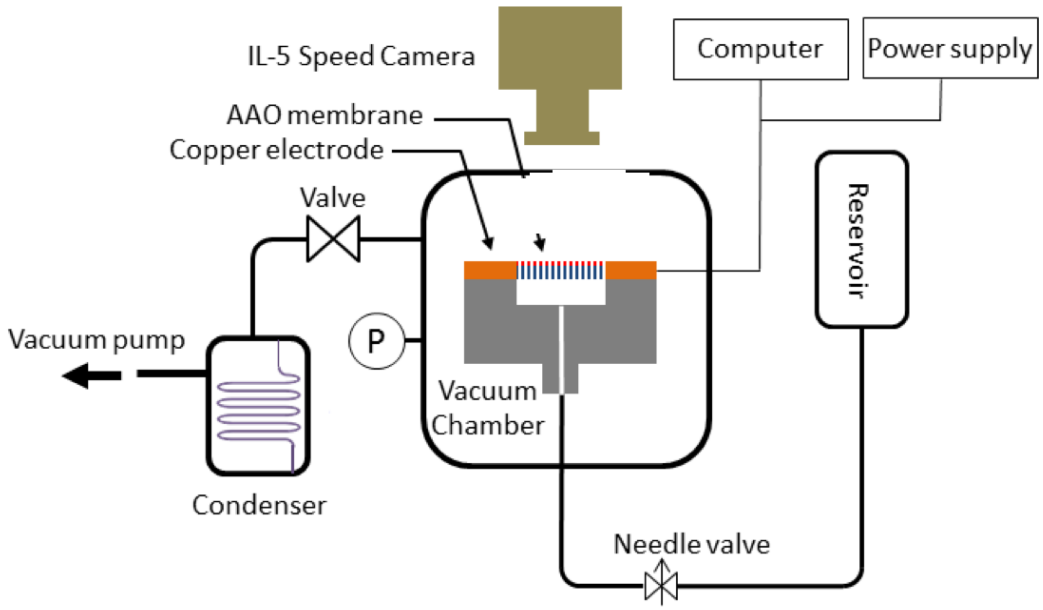

Figure 7: Complete diagram of the experimental set-up

The experiment was now able to begin. The power was increased in 5 W increments. At each step, the set-up reaches steady state after 10 seconds but was left under those conditions for 2 minutes to allow the system to come to a complete equilibrium and to record data. The heating power was continually increased until the membrane either dried out and/or broke.

Section III is currently being prepared for submission for publication of the material. Kim, Young Jin; Wang, Qingyang; McGrath, Kristine; Chen, Renkun.

IV. Experimental Results from Nanopore Evaporative Cooling Experiments

AAO membranes were purchased from the Supplier, Sigma Aldrich, Manufacturing Number Whatman, 6809-6022. The membranes purchased had an average pore size of 200 nm and a membrane thickness of 50 μm.

The working membrane was further characterized using an FEI XL30 SEM (Scanning Electron Microscope). It was determined from these images that the membrane pore sizes were ~200nm ±30nm and the porosity was ~0.52 using Image J.

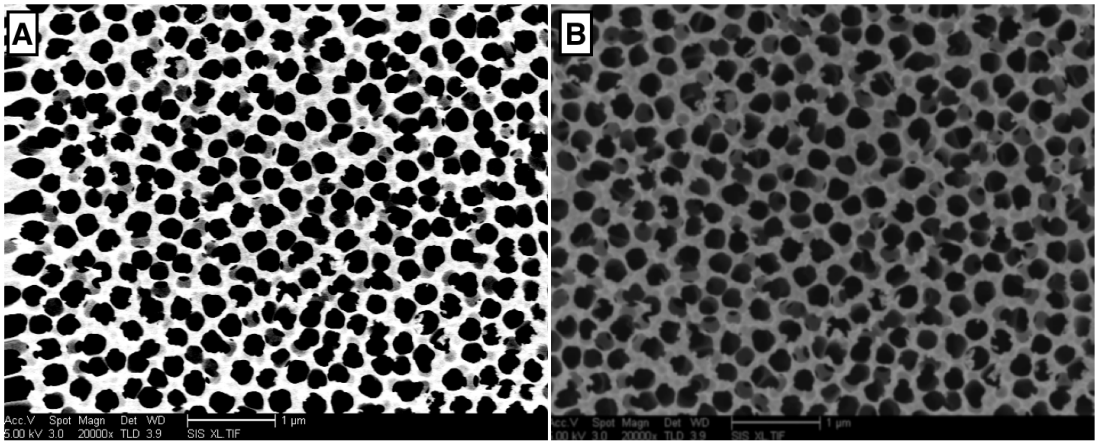

Figure 8: SEM image of the AAO membrane [A] before and [B] after Platinum was deposited. The membrane's pore size and porosity remained the same.

For a membrane with these parameters, a theoretical critical heat flux (CHF) of 572 W/cm^2 can be obtained, as discussed earlier. Experimentally, a maximum heat dissipation of 103 W on a 0.5 cm^2 area was achieved which corresponds to a heat flux of 206 W/cm^2 on the overall AAO surface or a heat flux of ~ 400 W/cm^2 if only the active evaporating pore area is taken into consideration.

Comparing these results to Xiao et al's results due to similarities in membrane material (AAO) and working fluid (IPA), a maximum heat flux of $\sim 96\, W/cm^2$ was dissipated [6]. The heat dissipation achieved in these experiments was two times greater than what Xiao was able to achieve and was much closer to the maximum theoretical critical heat flux namely, $\sim 570\, W/cm^2$ based on the pore area.

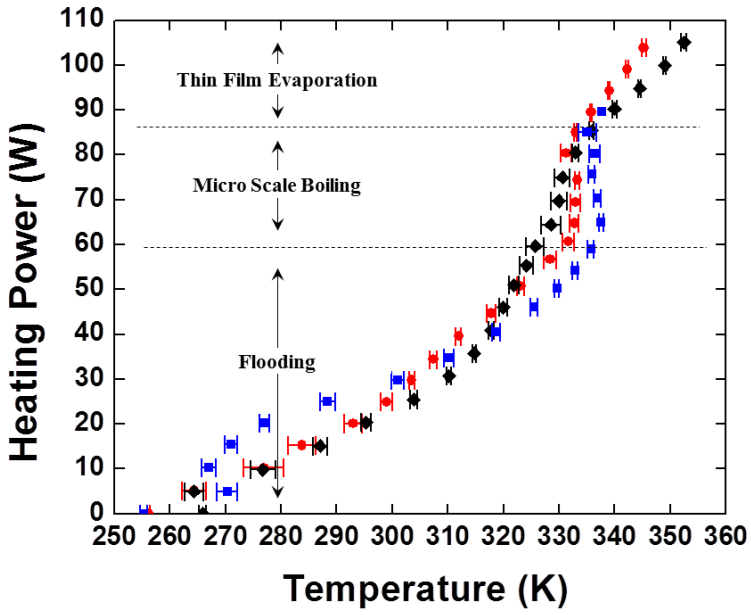

Figure 9: Experimental results using Whatman AAO membrane with a pore diameter of ~200 nm, membrane porosity of 52%, and a membrane thickness of 50 μm.

From the experiments and with the help of a high speed camera, the heat dissipation within the nanoporous membrane can be categorized into three regions prior to dryout. These regions are (1) flooding, (2) micro scale boiling, and (3) thin film evaporation. In previous works, it was only categorized into two regions, flooding and thin film evaporation [6], but with the use of a high definition, high speed camera

with a 1-5X magnifying macro lens, a resolution of 2 μm within the setup was achieved and an additional region called microscale boiling was observed and identified.

The first region is the flooding region. This region occurs at low superheats and is characterized by large temperature fluctuations for a given low heating power as shown in **Figure 10**. The reason for these temperature fluctuations is due to the flooding that occurred. The flooding was irregular and moved around as the membrane was heated.

As the heating power increased, heat dissipation switches to the microscale boiling and then eventually the thin film evaporating regime. These two regions are characterized by a steady temperature profile. The main difference between the two is that in the microscale boiling region, bubbles or boiling occurs. These bubbles appeared at a highest frequency of 250 Hz and had a size of less than 10 μm which cannot be observed by the human eye and was probably why it had not been identified previously. With the help of the high speed, high resolution camera, this region was able to be identified and observed. Also it can be seen that the temperature of the membrane remains relatively constant in this region even though the heating power is increasing as shown in **Figure 9**.

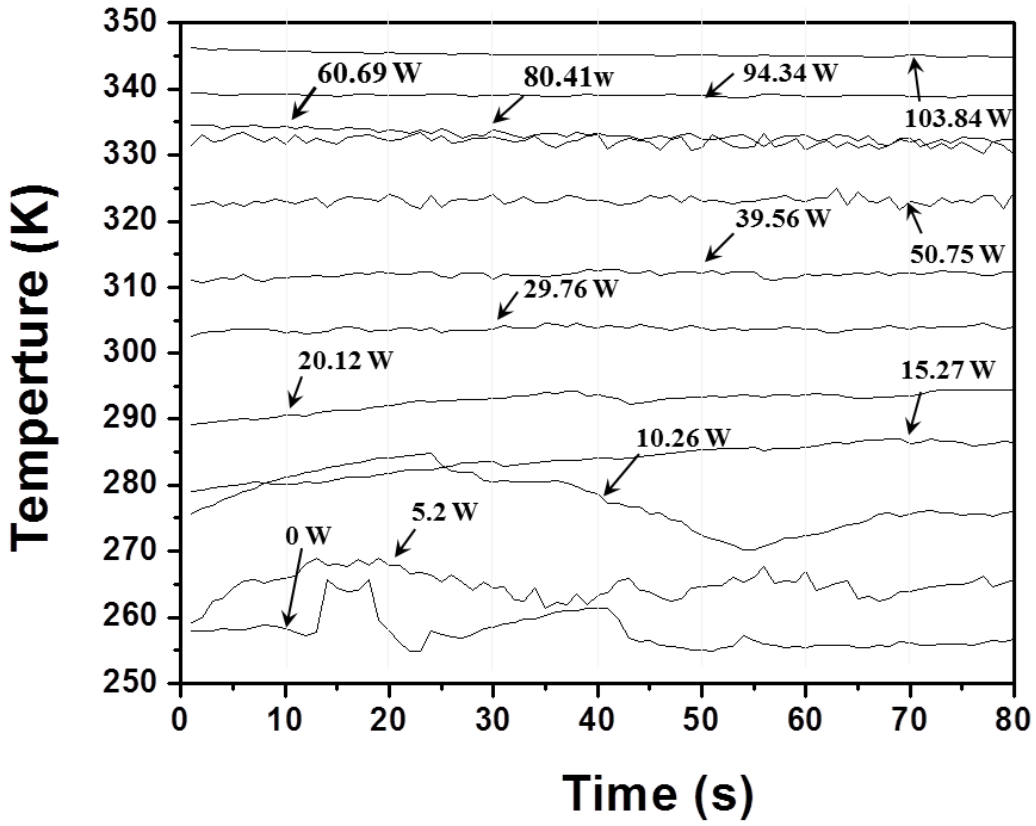

Figure 10: Temperature of the membrane with various heating powers. Large temperature fluctuations for a given heating power correlates to a membrane operating in the flooding regime. Steady temperature profiles for a given heating power correlates to a membrane operating in the micro boiling and thin film evaporation regime.

The results obtained from these experiments are very promising considering a heat flux much closer to the theoretical critical heat flux value was obtained. The experiments are limited by the variety of AAO that are commercially available which limits what parameters are able to be tested to obtain better experimental results and obtain higher heat flux dissipation. For this reason, the fabrication of AAO in the lab is required for future nanopore evaporative cooling experiments. By being able to

fabricate AAO in the lab, parameters such as membrane thickness, pore diameter, porosity, and pore ordering can be adjusted as necessary to better model and understand nanopore evaporative cooling.

Section IV is currently being prepared for submission for publication of the material. Kim, Young Jin; Wang, Qingyang; McGrath, Kristine; Chen, Renkun.

V. AAO Membrane

V.I Introduction

AAO has many uses in commercial product and industry such as mechanical and decorative coatings on aluminum, nanotechnology, and filtration [2-5]. Because of its diverse use, including both barrier and porous type AAO, much research has been done to better understand and control the properties of AAO. Barrier type AAO is produced using completely insoluble electrolytes while porous type is produced using slightly soluble electrolytes [29]. For the purposes of nanopore evaporative cooling, porous AAO membranes are required.

In the anodization process, the aluminum substrate is the anode and platinum is usually used as the cathode as shown in **Figure 11**. The aluminum atoms lose electrons through the current turning into Al^{3+}. The cations move toward the electrolyte-oxide interface while the anions move toward the oxide-aluminum interface when the voltage is applied [23] which leads to the growth of the AAO membrane. The chemical equation for the formation of AAO is [29]:

$$2Al(s) + 3H_2O(l) \rightarrow Al_2O_3(s) + 6H^+ + 6e^-$$

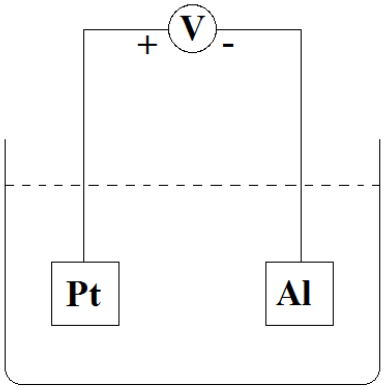

Figure 11: Anodization set-up

V.II Anodization Types

The most common anodization method is one-step [1] or two-step [3-4,17,21-22,24] direct current anodization. Both techniques are used but both have their own pros and cons, such as the fact that one-step anodization is much quicker than two-step anodization but it produces a non-uniform and disordered pore structure.

Other types of anodization methods that have been researched are hybrid pulse anodization [1], three-step anodization [16], and anodizing on a pre-patterned substrate [23]. While hybrid pulse anodization and three-step anodization have been shown to have a more ordered pore structure and produce more circular pores than two-step direct current anodization not much research has been done on them as of yet. For anodizing on a pre-patterned substrate, it also produces a more ordered pore structure but it limits the pore size that can be fabricated due to the fact that the mask

is pre-made and cannot be altered, only a new one can be made to obtain a different pore size.

Even within the two-step anodization process, there are two kinds of anodization processes: hard and mild. Mild anodization is formed at a lower current density while hard anodization is done at a higher current density which results in a faster oxide growth rate for the hard anodization, making it more cost effective and commercially viable [21-22]. Mild anodization also contains lower levels of anionic impurities compared to hard anodization [21].

The two-step anodization process is the most commonly used technique for AAO fabrication due to the fact that it produces better quality and more uniformly ordered pores than one-step anodization. During the first anodization step, the pores begin to form an ordered concave structure in the aluminum but the pores themselves are disordered. The oxide film formed by the first anodization is then completely etched away leaving behind an ordered pattern on the aluminum substrate. In this second anodization, because there is already a pre-patterned surface from the first anodization, the pores are able to use this pattern as a guide to form pores in a more ordered and uniform way.

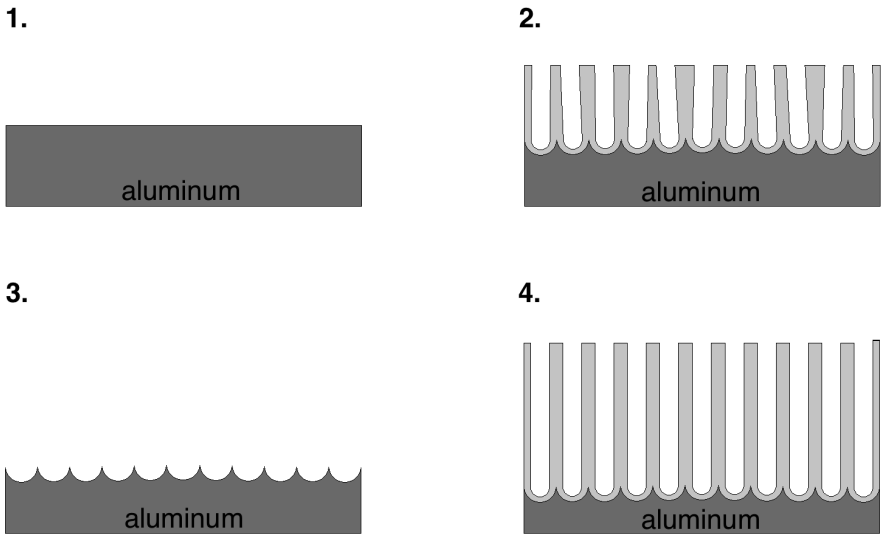

Figure 12: Two-step anodization. 1. The aluminum substrate. 2. First anodization. 3. Etching of the oxide layer formed during the first anodization. 4. Second anodization.

V.III Fabrication Parameters

From the various anodization methods and all the research that has been done, it has led to a better understanding of what fabrication parameters affect what membrane parameters such as pore uniformity, pore circularity, membrane thickness, pore size, and interpore distance.

The most common electrolytes used in the fabrication of AAO are sulfuric acid [20,22,30], oxalic acid [1,3,15-17,20-22,25,30,35], phosphoric acid [20,22,24,30], or a mixture involving them [4-5]. It has also been found through research that each solution has a certain voltage at which it produces the best ordered structure. For sulfuric acid it is 25 V [20,24,28,30], for oxalic acid it is 40 V [20,24,26,28,30], and for phosphoric acid it is 195 V [20,24,28,30]. At these conditions the pores sizes

produced are approximately 65 nm for sulfuric acid, 100 nm for oxalic acid, and 500 nm for phosphoric acid. Other less common electrolytes like citric acid [30] and malonic acid [28] have also been used. The electrolyte solution used during anodization effects the growth rate of the oxide, the barrier oxide thickness, and the voltage at which the best ordering occurs.

The aluminum substrate that the AAO is formed on also makes a difference to the quality of the AAO produced. High purity aluminum is most commonly used for AAO fabrication. It has been seen experimentally that the substrate purity effects the oxide growth rate, with the higher the purity the higher the growth rate [20]. High purity aluminum also produces AAO with a better pore size distribution and pore ordering than low purity aluminum [4].

The applied voltage during anodization has been shown to affect pore diameter, interpore distance, barrier oxide thickness, and wall thickness/porosity of the AAO [3-4,17,20,23,29]. However, as the applied voltage increases, the uniformity and ordering of the pore structure decreases due to dissolution effects.

The temperature of the electrolyte during anodization has a direct impact on the AAO growth rate. As the temperature increases so does the AAO growth rate. However, dissolution effects can occur at higher temperatures which is why many conventional AAO membranes are produced at low temperatures [1,3,15]. Pore size also increases with temperature but pore uniformity decreases.

The anodization time is directly related to the membrane thickness of the AAO produced. The membrane thickness increases with time. Process or anodization time also has a small effect on the barrier oxide layer thickness [20].

V.IV Aluminum Substrate Removal and Pore Opening/Widening

Once the growth of the AAO is complete, the aluminum substrate needs to be etched away along with the AAO barrier oxide layer in order to produce through holes. The aluminum substrate can be etched using a few different combination of solutions. The solutions used to etch the aluminum substrate away are a saturated $HgCl_2$ [17,20,23-24], a mixture of $CuCl_2$ and HCl [18,22,28,35], a mixture of $CuCl_2$, HCl, and DI water [21], and a saturated solution of $CuCl_2$ [25,27].

Once the aluminum substrate is etched away the barrier pores need to be removed in order to open the pores up and produce through holes. There are various solutions and techniques used to do this but the most popular technique is exposing the membrane to phosphoric acid [17-18,20,23-24].

Pore opening can also be done with dry etching techniques like ion milling and plasma etching but it is a complicated process, is only feasible for opening a small area of pores, and it requires expensive equipment to do so [18,20-22]. For the purposes of nanopore evaporative cooling experiments, the whole area of the AAO membrane needs to be opened which makes wet etching a more feasible option for this application due to the fact that it is cheaper and easier for a larger area.

Not only can the barrier pores be removed to open up the holes and make them through holes, but the pores can also be widened by further etching with the same solution. Pore widening is usually done as part of the process since the pore diameter is not easily controlled with the applied voltage alone. While this is a commonly used technique for pore opening and widening, it is controlled only by the etching time which has to be found experimentally since parameters such as temperature, concentration, and the thickness of the barrier layer of the AAO affect the rate at which it will open and widen. Because of this, there is a lot of inconsistency when pore opening and widening is done.

One solution to this problem is using electrochemical detection to determine when the pores are opened. This set-up involves using two electrodes and two half permeation cells that are separated only by the AAO membrane with the phosphoric acid solution in the permeation cell touching the barrier oxide side of the AAO and another solution such as KCl [18] or DI water [21] touching the front side of the AAO membrane so as not to destroy the ordered pores. A small voltage is then applied to the sample and the current is monitored. As the phosphoric acid begins to etch away the barrier oxide, the current is at its minimum and once the pores starts to open, the current then significantly increases.

VI. AAO Membrane Parameters for Evaporative Cooling

The nanopore evaporative cooling experiments first began with the use of Whatman produced AAO membranes with a 200 nm average pore size and a 50 μm membrane thickness. In order to better understand membrane parameters such as porosity, membrane thickness, and pore size, fabricating AAO in the lab was decided so that these parameters could be controlled and future experiments could be run to see how well the experimental data correlates with the theoretical data.

It was also decided to make AAO membranes due to the fact that commercial AAO is less ordered than what can be made in the lab [15] as shown in **Figure 13**. As can be seen in the SEM image, the pores are relatively similar in size when looking at it overall, however, when it is zoomed in the pore structure appears more disordered. The most notable aspect of the pores is that they are not very circular. Using Image J to analyze the images and the circularity equation:

$$Circularity = \frac{4\pi A}{P^2},$$

where A is the area of the pore and P is the perimeter of the pore, it can be calculated that the average circularity is 0.80 with a standard deviation of 0.073 based on 75 pores. A circularity value of 1 correlates to a perfect circle while a value that approaches 0 correlates to an increasingly elongated shape.

The average pore diameter can be found using the equation:

$$D = \frac{4A}{P},$$

where D is the average diameter of the pore. Using this equation, the average pore diameter was calculated to be 231.62 nm with a standard deviation of 22.94 nm.

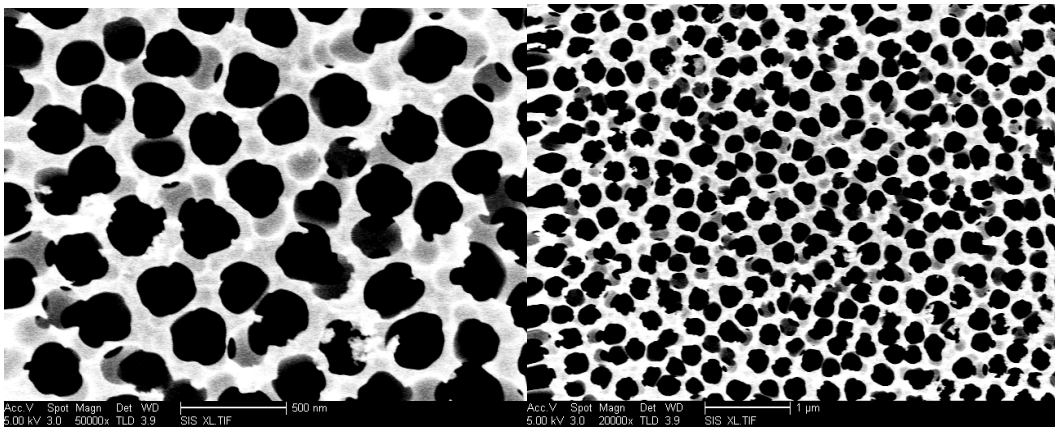

Figure 13: Front Side of Whatman Commercially Produced AAO

For the nanopore evaporative experiments, fabricating AAO membranes that are consistent in size and have a highly ordered pore structure is desired. For future experiments a variety of pore sizes and membrane thicknesses is also required.

VI.I Pore Size

The pore size can be changed by altering the applied voltage [15,17,20,25-26], electrolyte temperature [15,20], the concentration of sulfuric acid mixed in with oxalic acid [5], the electrolyte concentration [20], and the duration of the AAO growth process [3,15]. To increase the pore diameter, the electrolyte temperature, process duration, or applied voltage can be increased to do so.

The pore size is also affected and limited by the interpore distance. While the pore diameter itself has a few different parameters that can be tweaked to change its size, the interpore distance is only affected by the applied voltage, except in sulfuric acid. As the applied voltage increases so does the interpore distance [15,17,20,23]. And when sulfuric acid is used, an increasing electrolyte temperature results in an increasing interpore distance [20], but when oxalic acid or phosphoric acid are used, the temperature has no impact.

The pore size can be further increased at the very end of the AAO fabrication process in the pore opening and widening step. Phosphoric acid [17-18,23-24] can be used to etch away the pore walls of the AAO which effectively widen the pore diameter.

For the eventual purposes of nanopore evaporative cooling, pore sizes ranging from 20 nm to 800 nm is the goal. So far in literature the largest pore size achieved is 500 nm by anodizing aluminum in 0.3M phosphoric acid at 195V [20,24,28,30] and 600 nm by anodizing aluminum in 2M citric acid at 240V [30]. To achieve even higher pore diameters, the applied voltage will need to be increased even more so. However, as the applied voltage gets higher to produce larger pore sizes, the system can reach an upper voltage limit, the limit of which depends on factors such as the electrolyte solution and temperature, at which point the burning and breakdown of the AAO will occur [25,26].

For oxalic acid there has also been research to get even larger pore sizes with an increased voltage. However, at a certain voltage, burning and breakdown of the AAO has been a limiting factor as to how high of voltage that can be applied.

One solution to increase the upper voltage limit in oxalic acid is by forming an oxide layer at a lower voltage and then slowly increasing the voltage to the desired amount. With this method, a maximum of 215V can be achieved [26].

Another approach to further increase the voltage in oxalic acid is with a constant-current nonlinear voltage increasing process, the maximum voltage that can be applied in this scenario is 400 V [25]. The downside of this process is that the bottom of the membrane has disordered and branched pores. It is not until a certain point in the anodization process that steady, linear, and ordered pores begin to form. While this research may eventually be promising, the disordered and branched pore layer is undesirable for this application since it cannot be easily removed without destroying the ordered linear portion of the AAO membrane.

VI.II Membrane Thickness

Membrane thickness is altered directly by changing the amount of anodization time. However, the growth rate of the AAO changes with the electrolyte, electrolyte temperature, and the aluminum substrate purity.

For future nanopore evaporative cooling experiments, membrane thicknesses ranging from 10 μm to 50 μm are desired. While easy to control the thickness, the

AAO membranes with thin thicknesses are difficult to manufacture due to the fact that they are very brittle and do not have much structural integrity once the aluminum substrate is etched away, making it more challenging to produce AAO at the lower end of the desired membrane thicknesses.

VI.III Pore Ordering

Pore ordering and uniformity is affected by the electrolyte temperature, the length of the first step of the anodization process [3,16], the applied voltage [3], and the aluminum substrate purity. Pore ordering decreases with higher electrolyte temperatures, a shorter first step anodization, a higher applied voltage, or a lower aluminum substrate purity.

The pore ordering is also affected by the number of anodization steps. Two-step anodization produces more ordered and uniform pore arrangements than one-step anodization. Not much research has been done into three-step anodization, but from the research that has been done so far, the pores are even more uniform [16].

VII. Experimental Design for AAO Fabrication

VII.I Introduction

Before AAO membranes with a variety of pore sizes and thicknesses can be fabricated, the process of fabricating generic and workable AAO has to first be solidified. AAO is best produced in 0.3M oxalic acid at 40V at low temperatures [3,15,17]. Using these set parameters, the fabrication of AAO in the lab can be fine-tuned to show that it is in fact feasible before more time and research are put into adjusting the parameters to obtain various membrane thicknesses, pore sizes, porosities, and better ordering.

VII.II AAO Fabrication Set-up

An aluminum substrate was used to fabricate the AAO membrane. The aluminum substrate was cut to 25mm x 25mm with a 0.2mm thickness. The substrate was then cleaned with IPA and allowed to air dry. The substrate was then set in a solution of NaOH for one minute and rinsed off with DI water. The aluminum substrate was then electropolished in perchloric acid at 20V for 5 minutes at 6-7℃. After, the sample was placed in two ethanol baths and then allowed to air dry.

Next, the sample was anodized in 0.3M Oxalic acid at 6-7℃ at 40V for one hour and then placed in two DI water baths and air dried. The sample was then placed in a bath of 6wt% H_3PO_4 + 1.8wt% H_2CrO_4 at 65℃ for 1 hour to etch away the oxide layer grown in the first step. The sample was then cleaned in DI water and then IPA.

The sample was then anodized again in the same 0.3M Oxalic acid at 6-7℃ at 40V for a predetermined time depending on how thick of membrane is desired and then placed in two DI water baths and allowed to air dry.

Next the aluminum substrate was etched away by placing the aluminum side of the sample on top of the solution so that it is floating on the liquid. After the aluminum was completely etched away, the barrier oxide AAO on the bottom needs to be etched away in order to open the pores to have through holes using phosphoric acid.

VIII. Results and Analysis of AAO Fabrication

VIII.I AAO Sample Holders

The fabrication of AAO in the lab first began with a simple design as shown below. It involved using copper tape, insulation tape, and Microshield Stop-off Lacquer red paint to cover the back of the aluminum substrate and prevent leaks from occurring during the electropolishing and anodization steps. This paint design has been used in various AAO fabrication set-ups [3,15].

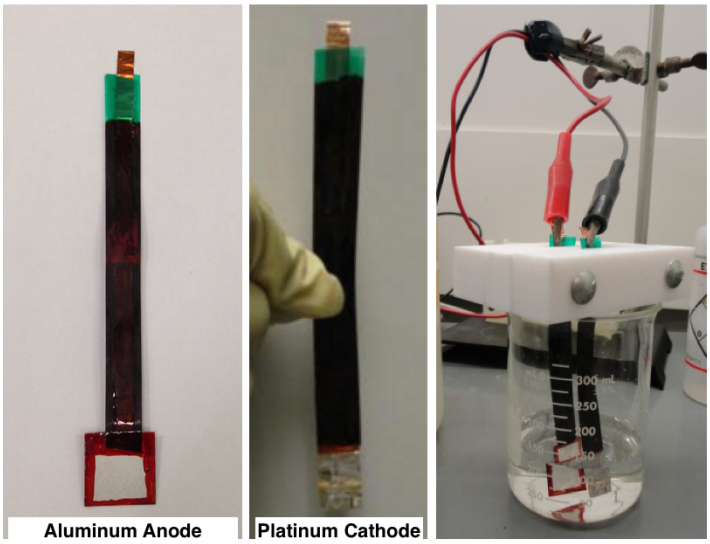

Figure 14: Initial AAO fabrication set-up.

However, using the Microshield Stop-off Lacquer red paint caused contamination on the AAO membrane when it was removed after the second anodization step prior to the aluminum etching, as shown in **Figure 15**. This residue is undesirable for AAO fabrication and nanopore evaporative cooling.

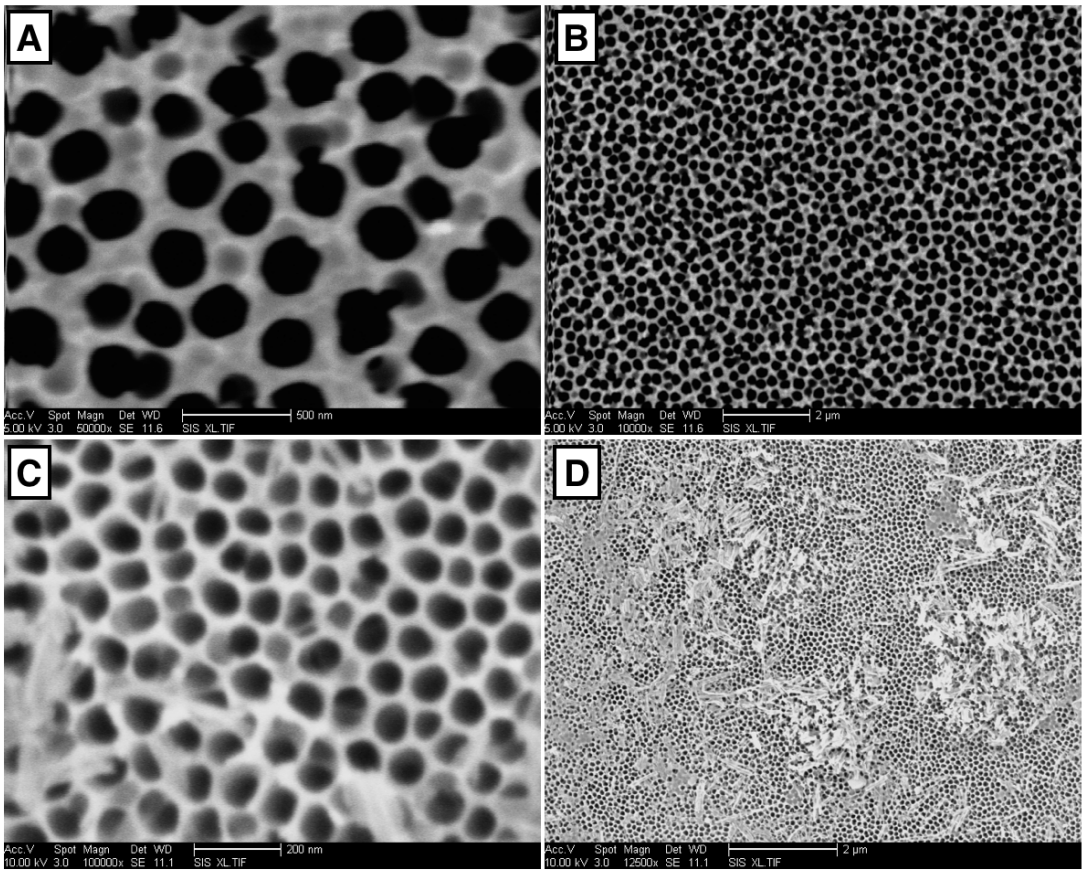

Figure 15: SEM images of AAO with initial set-up. Top photos (A&B) are after 1-step anodization. Bottom photos (C&D) are after 2-step anodization. Paint residue can be seen on the AAO membrane.

Looking closely at the SEM images, not much residue can be seen after the first anodization step due to the fact that the paint has not been removed from the aluminum substrate. After the second anodization and the removal of the paint, however, it can be clearly seen in the SEM images that the paint was not fully removed even though it appeared to be when looking at it with the human eye.

To prevent this undesired residue from the paint, a new experimental set-up was made. This new set-up involves using an acrylic fixture for insulation rather than the Microshield Stop-off Lacquer red paint as shown below.

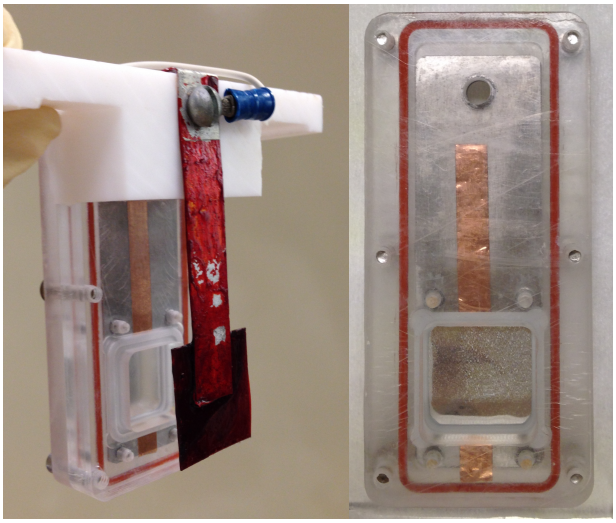

Figure 16: Current experimental set-up for AAO fabrication.

In this new set-up, two different acrylic fixtures are used, one for the electropolishing step and one for the anodization steps. The first fixture has a 0.87 in x 0.87 in size opening for the aluminum substrate and the second has a 0.75 in x 0.75 in size opening for the substrate as shown in **Figure 17**. This is done in order to ensure all the aluminum being anodized is electropolished which produces a better quality AAO especially on the edges where the aluminum meets the acrylic fixture since the substrate has to be moved in and out of the fixtures a few times during the process.

In this new set-up it is placed in the first fixture for electropolishing. It is then removed from this fixture into the second fixture that has a slightly smaller opening

for the first anodization. After, the aluminum substrate is removed from this fixture and placed directly into the 6wt% H_3PO_4 + 1.8wt% H_2CrO_4 bath. Then, it is placed in the second fixture once again to undergo a second anodization.

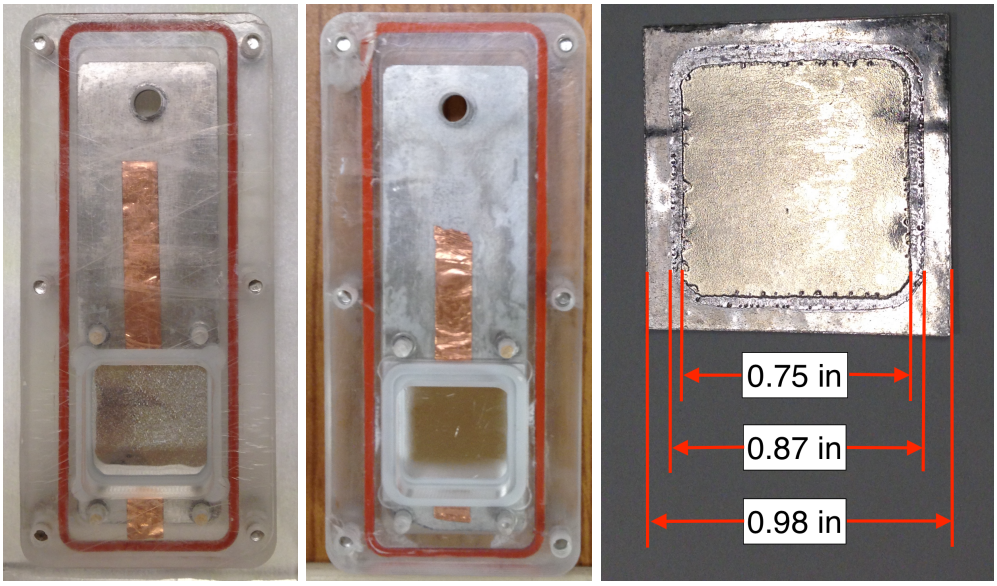

Figure 17: Fixture designs for AAO fabrication and AAO produced on aluminum substrate.

After extended use, the acrylic sample holders become damaged from the electropolishing step in the perchloric acid. The once transparent sample holder becomes cloudy and holes/cracks form resulting in leaks in the sample holder which is undesirable. To combat this issue, the aluminum sample is no longer electropolished in a fixture but instead directly electropolished as is and then cut in size to 0.98 in x 0.98 in to fit in the sample holder used for anodization.

VIII.II High Purity Vs Low Purity Aluminum for the Fabrication of AAO

AAO fabrication was done with both high purity aluminum 99.997% and low purity aluminum 99.99% to see which produced the best results and workable membranes for future experiments.

The front side of the AAO produced with low purity aluminum produced acceptable results. Analyzing over 1,000 pores, the average circularity was calculated as 0.89 with a standard deviation of 0.033 and the average pore size was calculated as 87.83 nm with a standard deviation of 4.02 nm. The backside, however, formed nano wires when the barrier oxide AAO was etched away which is undesirable and unacceptable for future use.

From the low purity experiments, it was also seen that with extended pore opening/widening time, the pores became even more disordered and the quality was worse as seen in **Figure 18 (C and D).**

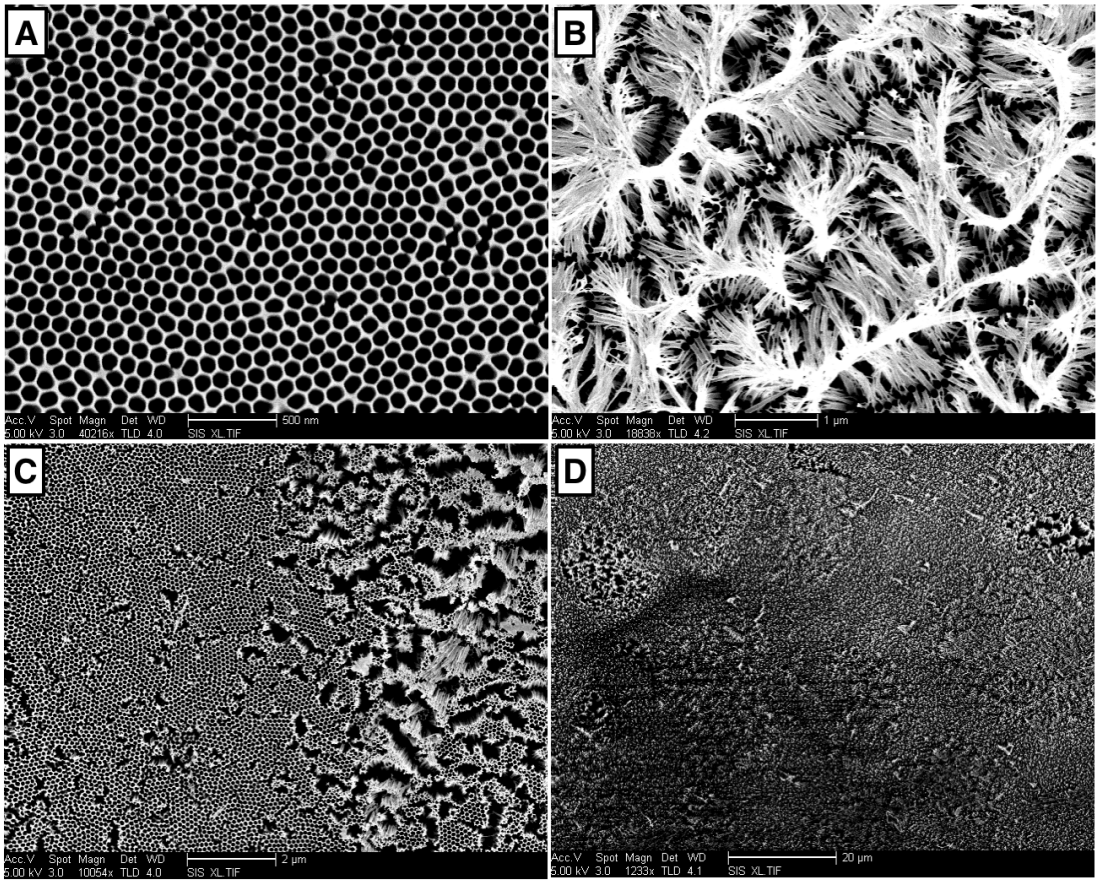

Figure 18: Low purity aluminum (99.99%) for the fabrication of AAO. A. Front side of AAO with pore opening done for 2 hours. B. Back side of AAO with pore opening done for 2 hours. C. Front side of AAO with pore opening done for 4 hours. D. Back side of AAO with pore opening done for 4 hours.

The high purity aluminum substrates produced AAO as seen in **Figure 19**. It can clearly be seen just from the images alone that the AAO produced with the high purity aluminum is much more ordered and has better quality than the low purity aluminum, especially on the backside of the AAO. For the front side of the AAO membrane, the average circularity is 0.91 with a standard deviation of 0.049 and an

average pore diameter of 83.10 nm with a standard variation of 3.44 based on over 500 pores.

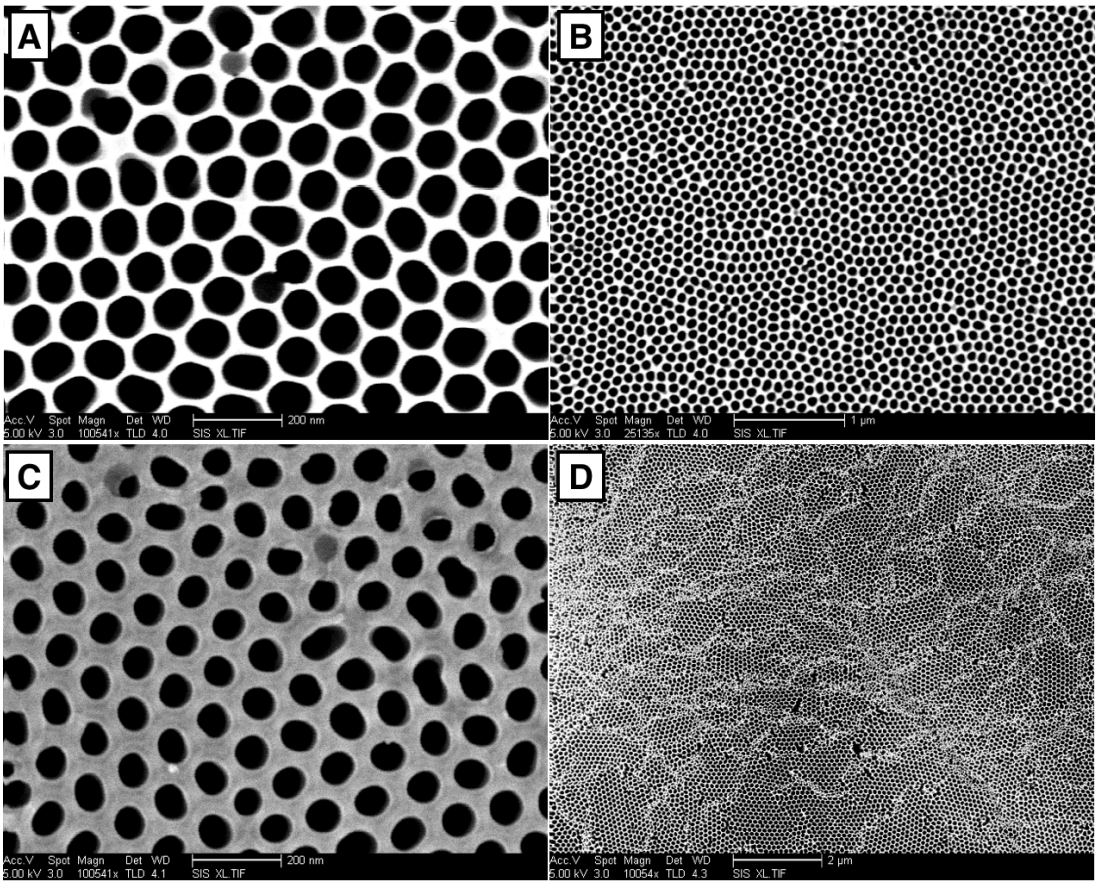

Figure 19: High purity aluminum (99.997%) for the fabrication of AAO with pore opening done for 1.5 hours. Front side of AAO (A&B). Back side of AAO (C&D).

From these calculations, it can be seen that the higher purity aluminum has a higher pore circularity than the low purity aluminum. Also it has a tighter pore size distribution and a smaller average pore diameter for the front side of the AAO. When the backside of the AAO is compared, the pores are clearly better in the high purity

aluminum just by looking at the images alone. The pores cannot even be distinguished in the low purity aluminum since nanowires have formed.

VIII.III Aluminum Substrate Etching and Pore Opening/Widening

Once the AAO growth part of the fabrication process was solidified, the aluminum etching and pore opening/widening still needed to be addressed. The aluminum substrate was originally etched away in a 1:1:1 solution of 0.2M $CuCl_2$, HCl, and DI water with the sample placed on top of the solution so that it was floating on top of the liquid. With this solution however, the HCl portion of the solution would produce a significant amount of bubbles causing the aluminum substrate to vibrate as the bubbles would move to the outer edge of the substrate to be released. These bubbles also caused the aluminum substrate to be etched away unevenly causing parts of the membrane to still have aluminum on them while other parts started to have the barrier oxide layer of the AAO prematurely removed as seen in **Figure 20.A.**

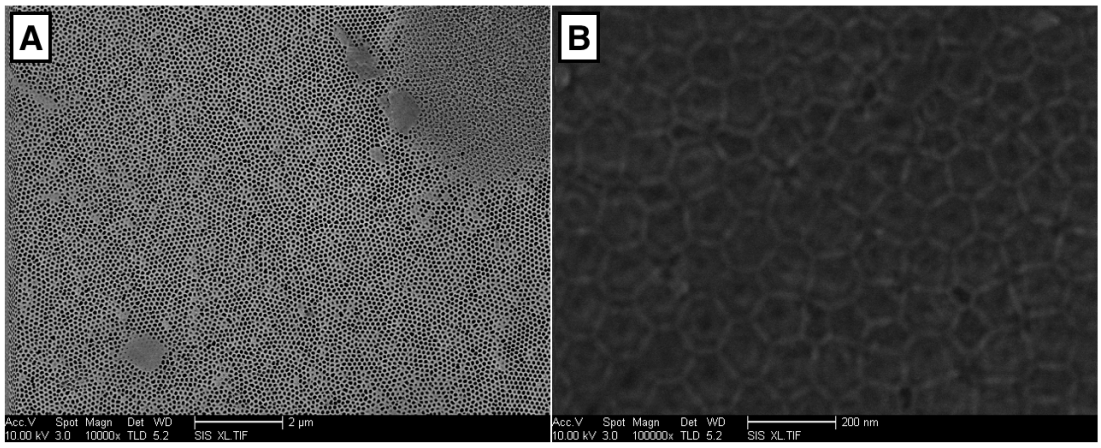

Figure 20: Back side of AAO after aluminum substrate etching using 1:1:1 solution of 0.2M $CuCl_2$, HCl, and DI water. A. SEM image showing uneven etching of the aluminum substrate. B. SEM image showing ideal backside of AAO. Barrier pores should be visible.

At this point in the fabrication process, all the barrier pores should still be visible as shown in **Figure 20.B**. The aluminum substrate etching step should only be removing the aluminum but not opening any of the pores yet.

To combat this issue, a solution of 0.4M $CuCl_2$ is used to etch away the aluminum substrate. The difference in the quality of the AAO with the different solutions can be seen in **Figure 21**. While the change in solution does produce better quality results especially after the pore opening step, they are still not quite the results desired here. This is because the aluminum substrate is still not being removed uniformly resulting in prematurely opened pores. There are not as many as was seen in the previous solution used but it is still not ideal.

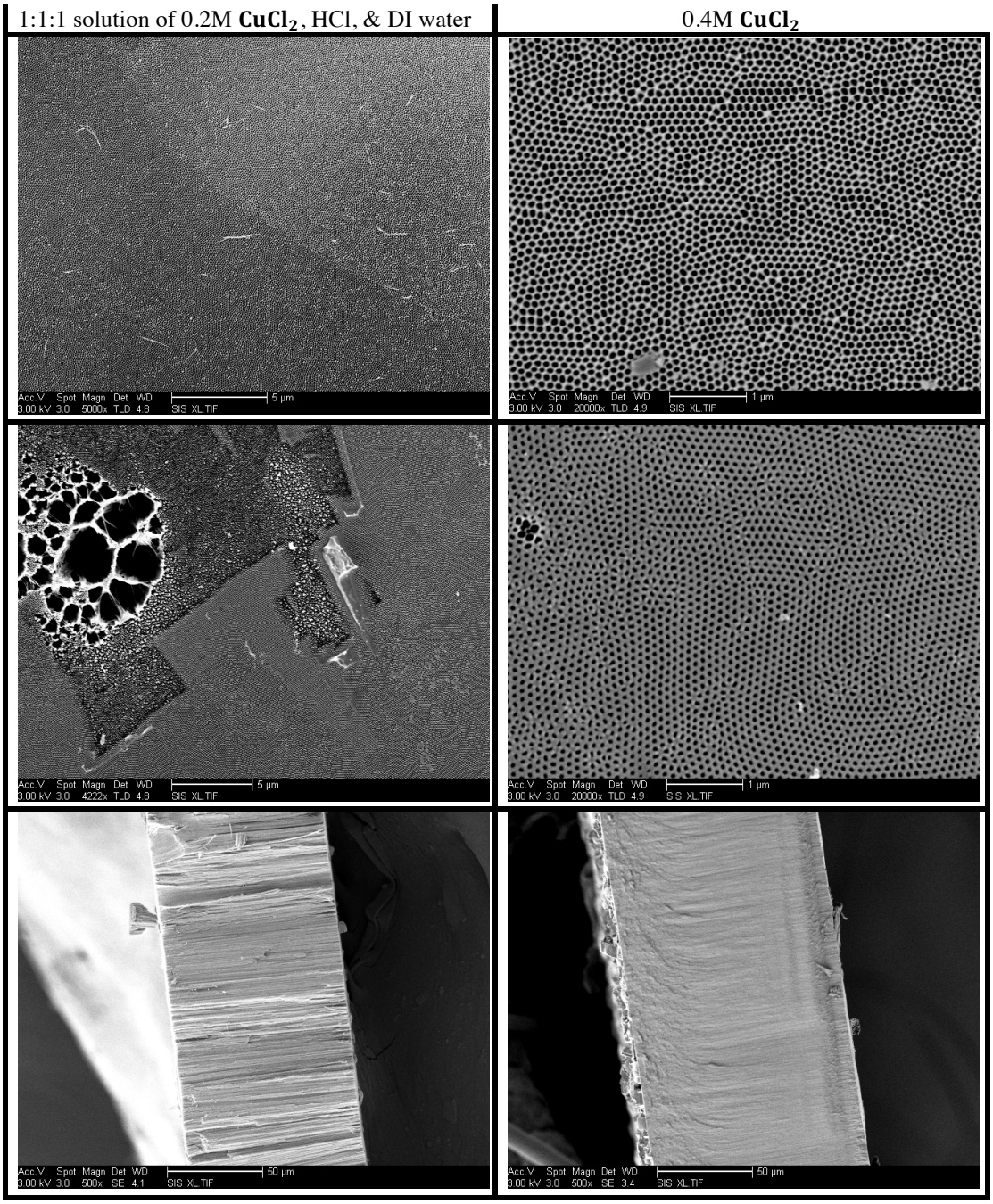

Figure 21: A comparison between etching with a 1:1:1 solution of 0.2M $CuCl_2$, HCl, and DI water with pore opening done for 2.5 hours and etching with a solution of 0.4M $CuCl_2$ with pore opening done for 1.75 hours. Top photos are the front side of the AAO. Middle photos are the back side of the AAO. Bottom photos are the side view of the AAO.

Since the solution of 0.4M $CuCl_2$ was not quite right, a solution of pure $CuCl_2$ was used to etch away the aluminum substrate and the results of which can be seen in **Figure 22**. With this new solution, there is no premature pore opening and the barrier oxide pores are visible which is what it should look like at this stage. However, zooming out on the SEM image of the membrane, a residue can be seen.

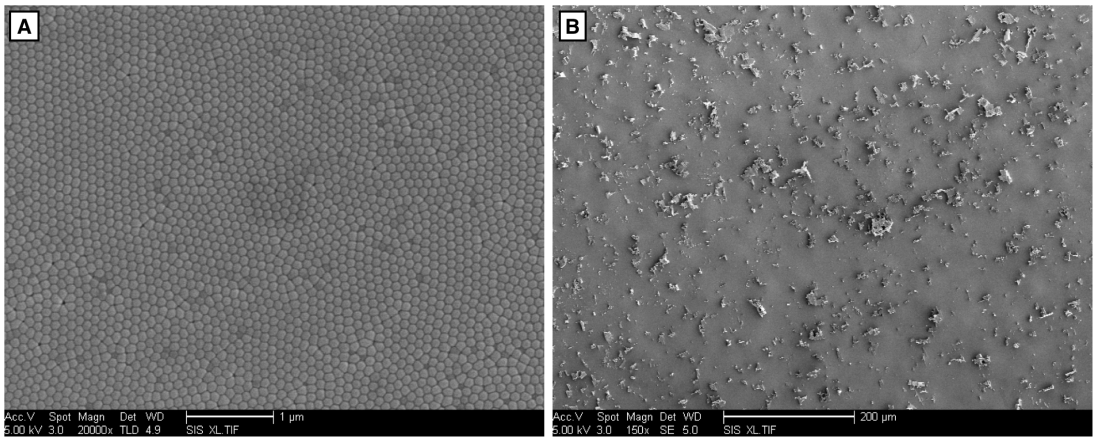

Figure 22: Aluminum substrate etched with pure $CuCl_2$. A. High magnification of back side of AAO. B. Low magnification of back side of AAO.

To open the bottoms of the pores for this experiment, the AAO was floated barrier oxide layer face down on the liquid and kept there until the pores opened. This was signified by the AAO membrane sinking upon pore opening. This would occur because the AAO membrane would float until the pores were open and the capillary pressure would bring the liquid into the nanopores causing it to sink. Upon inspection of the nanopores with the SEM, it can be seen and calculated that the pores on the bottom while open are not completely open as shown in **Figure 23**. They have an

average diameter of 67.91 nm with a standard deviation of 3.69 compared to the top that has an average diameter of 82.29 nm.

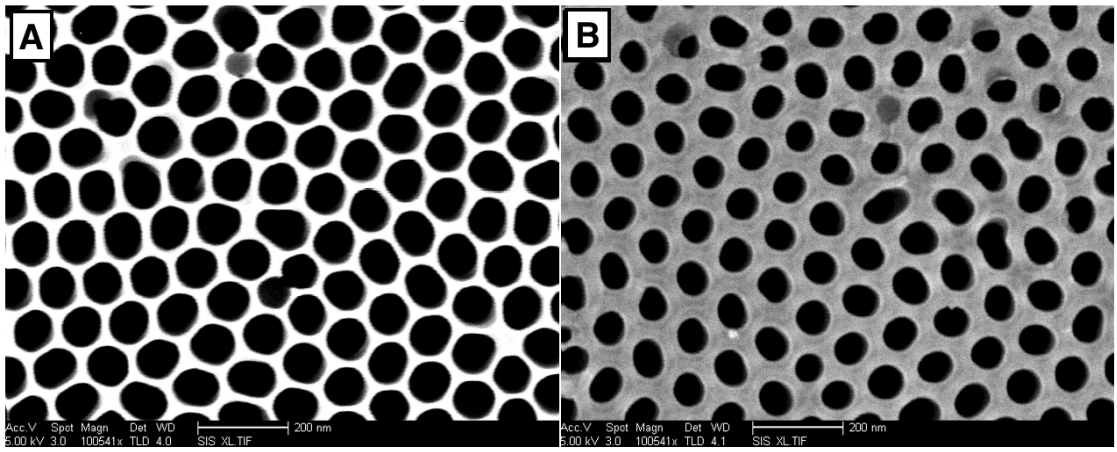

Figure 23: Images of AAO after pore opening done until the membrane sank in the solution. A. Front side of AAO. B. Back side of AAO.

In order to get uniform through holes, the membrane would need to be left in the solution for a few minutes longer to finish opening the pore but not destroy the pore structure as seen in **Figure 24.**

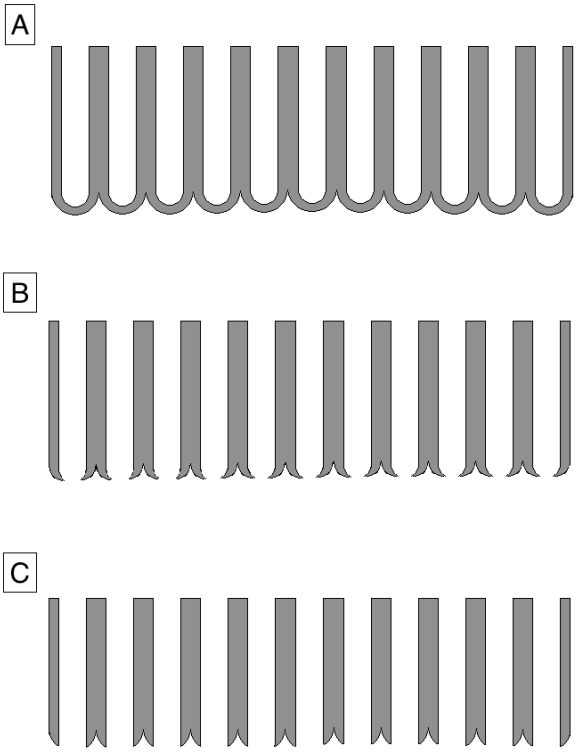

Figure 24: Pore opening. A. Barrier oxide pores prior to opening, after aluminum substrate etching. B. Initial pore opening. C. Pores all the way opened.

VIII.IV Membrane Thickness

To begin with, AAO was produced with 0.3M Oxalic acid at 6-7℃ at 40V with the first anodization step lasting 1 hour and the second step lasting 16 hours to produce a thicker and stronger membrane to work with to solidify the AAO process steps. Under these conditions, the AAO membranes produced have an average pore size of 80 nm and a thickness of 100μm.

However, the Whatman AAO membranes have a thickness of 50 μm that we want to replicate to make the AAO membranes more comparable. In order to do that,

the second step anodization was changed from 16 hours to 8 hours since the AAO growth rate was found to be ~6.25 $\mu m/hour$.

IX. Conclusion

For the nanopore evaporative cooling experiments a great improvement in the experimental results was shown. For a membrane with the parameters used, a theoretical critical heat flux (CHF) of 572 W/cm^2 can be obtained. Experimentally, a maximum heat dissipation of 103 W on a 0.5 cm^2 area, corresponding to a heat flux of 206 W/cm^2 on the overall AAO surface or a heat flux of ~ 400 W/cm^2 on the active evaporating pore area was achieved showing that there is promise to achieving even higher heat dissipation. In order to do this however, AAO with various working parameters need to be tested to better understand and model this. With the commercially produced AAO, nanopore evaporative cooling experiments are very limited in what can be tested. For this reason and the fact that commercial AAO is not well ordered, the fabrication of AAO in the lab was done.

Using an acrylic fixture design, the AAO fabrication has been solidified in 0.3M oxalic acid at 40V at a low temperature of 6-7℃ using $CuCl_2$ to etch the aluminum and phosphoric acid to open the pores. Using these set parameters to fine tune the fabrication of AAO, AAO with ~80 nm in size is produced.

With both the high and low purity aluminum used in the lab, more ordered pores were produced compared to the store purchased AAO when looking at the front side of the AAO. A circularity of 0.91 was achieved for the AAO produced on high purity aluminum and a circularity of 0.89 was achieved for the AAO produced on low purity aluminum, while the commercially produced AAO had only a circularity of 0.80. However, when looking at the back side of the AAO, the low purity aluminum

produced nano wires after the pore opening/widening step which is undesirable and unusable. Therefore, the high purity aluminum has to be used to produce workable AAO membranes.

With the set-up and fabrication conditions, it was calculated that the AAO growth rate was ~6.25 $\mu m/hour$. For the purposes of future nanopore evaporative cooling experiments, membranes with thicknesses of 10, 30, ad 50 μm are required. The growth of the AAO itself it easy to control with no real issues. However, removing the aluminum substrate and opening/widening the pores for a thinner AAO membrane without damaging it will be a challenge due to a lack of mechanical strength.

Membranes with pore sizes of 20, 200, and 800 nm, while having highly ordered pores are also a requirement. To get these parameters, process conditions such as applied voltage, electrolyte, electrolyte concentration, solution temperature, and anodization time can be altered to obtain them. In the research done so far, the highest pore size achieved was 600 nm with 2M citric acid at 240V. So to reach the higher limit on the pore diameter, the applied voltage and the electrolyte used will need to be changed for future membrane fabrication. While 600 nm is close to the desired upper limit on pore sizes wanted for future experiments, it is still not quite there. Further research and experiments still needs to be done to fine tune these parameters especially in order to get pore diameters that big and membrane thicknesses that small without breaking them.

Bibliography

[1] Chung, C. K.; Liao, M. W.; Chang, H. C.; & Lee, C. T. (2011). Effects of Temperature and Voltage Mode on Nanoporous Anodic Aluminum Oxide Films by One-step Anodization. *Thin Solid Films, 520,* 1554-1558.

[2] Oh, J. & Thompson, C V. (2011). The Role of Electric Field in Pore Formation during Aluminum Anodization. *Electrochimica Acta, 56,* 4044-4051.

[3] Stepniowski, W. J. & Bojar, Z. (2011). Synthesis of Anodic Aluminum Oxide (AAO) at Relatively High Temperatures. Study of the Influence of Anodization Conditions on the Alumina Structural Features. *Surface and Coatings Technology, 206,* 265-272.

[4] Michalska-Domanska, M.; Norek, M.; Stepniowski, W. J.; & Budner, B. (2013). Fabrication of High Quality Anodic Aluminum Oxide (AAO) on Low Purity Aluminum- A Comparative Study with the AAO Produced on High Purity Aluminum. *Electrochemica Acta, 105,* 424-432.

[5] Bai, A.; Hu, C.; Yang, Y.; & Lin, C. (2008). Pore Diameter Control of Anodic Aluminum Oxide with Ordered Array of Nanopores. *Electrochimica Acta, 53,* 2258-2264.

[6] Xiao, R.; Marro, S. C.; & Wang, E. N. (2013). Negative Pressures in Nanoporous Membranes for Thin Film Evaporation. *Applied Physics Letters, 102,* 123103.

[7] Lu, Z. (2014). *Design and Modeling of a High Flux Cooling Device Based on Thin Film Evaporation from Thin Nanoporous Membranes*. Boston: Massachusetts Institute of Technology.

[8] Plawsky, J. L.; Fedorov, A. G.; Garimella, S. V.; Ma, H. B.; Maroo, S. C.; Chen, L.; & Nam, Y. (2014). Nano- and Microstructures for Thin-film Evaporation—A Review. *Taylor & Francis, 18,* 251-269.

[9] Narayanan, S.; Fedorov, A. G.; & Joshi, Y. K. (2011). Interfacial Transport of Evaporating Water Confined in Nanopores. *Langmuir, 27,* 10666-10676.

[10] Hu, H.; Weinberger, C. R.; & Sun, Y. (2014). Effect of Nanostructures on the Meniscus Shape and Disjoining Pressure of Ultrathin Liquid Film. *Nano Letters, 14,* 7131-7137.

[11] Kaplan, F.; De Vivero, C.; Howes, S.; Arora, M.; Homayoun, H.; Burleson, W.; Tullsen, D.; & Coskun, A. K. (n.d.). Modeling and Analysis of Phase Change Materials for Efficient Thermal Management. 1-8.

[12] Zou, A.; Chanana, A.; Agrawal, A.; Wayner, P. C.; & Maroo, S. (2016). Steady State Vapor Bubble in Pool Boiling. *Scientific Reports,* 1-8.

[13] Coso, D.; Srinivasan, V.; Lu, M.; Chang, J.; & Majumdar, A. (2012). Enhanced Heat Transfer in Biporous Wicks in the Thin Film Evaporation and Boiling Regimes. *Journal of Heat Transfer, 134,* 101501.

[14] Lu, Z.; Narayanan, S.; & Wang, E. N. (2015). Modeling of Evaporation from Nanopores with Nonequilibrium and Nonlocal Effects. *Langmuir, 31.* 9817-9824.

[15] Sulka, G. D. & Stepniowski, W. J. (2009). Structural Features of Self-Organized Nanopore Arrays Formed by Anodization of Aluminum in Oxalic Acid at Relatively High Temperatures. *Electrochimica Acta, 54,* 3683-3691.

[16] Nasirpouri, F.; Abdollahzadeh, M.; Almasi, M. J.; & Parvini-Ahmadi, N. (2009). A Comparison between Self-ordering of Nanopores in Aluminum Oxide Films Achieved by Two- and Three-step Anodic Oxidation. *Current Applied Physics, 9,* S91-S94.

[17] Wang. X. & Han, G. (2003). Fabrication and Characterization of Anodic Aluminum Oxide Template. *Microelectronic Engineering, 66,* 166-170.

[18] Lillo, M. & Losic, D. (2009). Pore Opening Detection for Controlled Dissolution of Barrier Oxide Layer and Fabrication of Nanoporous Alumina with Through-hole Morphology. *Journal of Membrane Science, 327,* 11-17.

[19] Zhao, X.; Seo, S.; Lee, U.; & Lee, K. (2007). Controlled Electrochemical Dissolution of Anodic Aluminum Oxide for Preparation of Open-Through Pore Structures. *Journal of the Electrochemical Society, 154,* C553-C557.

[20] Zaraska, L.; Sulka, G. D.; & Jaskula, M. (2011). Anodic Alumina Membranes with Defined Pore Diameters and Thicknesses Obtained by Adjusting the Anodizing Duration and Pore Opening/Widening Time. *J Solid State Electrochem, 15,* 2427-2436.

[21] Han, H.; Park, S.; Jang, J. S.; Ryu, H.; Kim, K. J.; Baik, S.; & Lee, W. (2013). *In Situ* Determination of the Pore Opening Point during Wet-Chemical Etching of the Barrier Layer of Porous Anodic Aluminum Oxide: Nonuniform Impurity Distribution in Anodic Oxide. *Applied Materials & Interfaces, 5,* 3441-3448.

[22] Lillo, M. & Losic, D. (2009). Ion-beam Pore Opening of Porous Anodic Alumina: The Formation of Single Nanopore and Nanopore Arrays. *Materials Letters, 63,* 457-460.

[23] Lu, C. & Chen, Z. (2011). Anodic Aluminum Oxide—Based Nanostructures and Devices. *Encyclopedia of Nanoscience and Nanotechnology, 11,* 235-259.

[24] Masuda, H.; Yada, K.; & Osaka, A. (1998). Self-ordering of Cell Configuration of Anodic Porous Alumina with Large-Size Pores in Phosphoric Acid Solution. *Japanese Journal of Applied Physics, 37,* L1340-L1342.

[25] Yi, L.; Zhiyuan, L.; Xing, H.; Yisen, L.; & Yi, C. (2011). Formation and Microstructures of Unique Nanoporous AAO Films Fabricated by High Voltage Anodization. *Journal of Materials Chemistry, 21,* 9661-9666.

[26] Yi, L.; Zhiyuan, L.; Shuoshuo, C.; Xing, H.; & Xinhua, H. (2010). Novel AAO Films and Hollow Nanostructures Fabricated by Ultra-High Voltage Hard Anodization. *ChemComm, 46,* 309-311.

[27] Yi, L.; Zhiyuan, L.; Shuoshuo, C.; Xing, H.; & Xinhua, H. (2010). Novel AAO Films and Hollow Nanostructures Fabricated by Ultra-High Voltage Hard Anodization—Supporting Information. *Supplementary Material (ESI) for Chemical Communications*.

[28] Lee, W.; Nielsch, K.; & Gosele, U. (2007). Self-ordering Behavior of Nanoporous Anodic Aluminum Oxide (AAO) in Malonic Acid Anodization. *Nanotechnology, 18,* 475713.

[29] Choi, J. (2004) Fabrication of Monodomain Porous Alumina Using Nanoimprint Lithography and its Applications.

[30] Ono, S.; Saito, M.; Ishiguro, M.; & Asoh, H. (2004). Controlling Factor of Self-Ordering of Anodic Porous Alumina. *Journal of the Electrochemical Society, 151,* B473-B478.

[31] Palko, J. W.; Zhang, C.; Wilbur, J. D.; Dusseault, T. J.; Asheghi, M.; & Goodson, K. E. (2015). Approaching the Limits of Two-Phase Boiling Heat Transfer: High Heat Flux and Low Superheat. *Applied Physics Letters, 107,* 253903.

[32] Semenic, T. & Cotton, I. (2009). Experimental Study of Biporous Wicks for High Heat Flux Applications. *International Journal of Heat and Mass Transfer, 52,* 5113-5121.

[33] Carey, V. P. (1992). *Liquid-Vapor Phase-Change Phenomena* (2 ed.). New York: CRC Press.

[34] Narayanan, S.; Fedorow, A. G.; & Joshi, Y. K. (2013). Heat and Mass Transfer during Evaporation of Thin Liquid Films Confined by Nanoporous Membranes Subjected to Air Jet Impingement. *International Journal of Heat and Mass Transfer, 58,* 300-311.

[35] Zhao, Y.; Chen, M.; Zhang, Y.; Xu, T.; & Liu, W. (2005). A Facile Approach to Formation of Through-hole Porous Anodic Aluminum Oxide Film. *Materials Letters, 59,* 40-43.